Single-sided acoustic beam splitting based on parity-time symmetry

Tuo Liu [1], Guancong Ma [2], Shanjun Liang [1,3], He Gao,[1] Zhongming Gu,[1] Shuowei An,[1] and Jie Zhu [1,*]

[1]*Department of Mechanical Engineering, Hong Kong Polytechnic University, Hong Kong SAR, China*
[2]*Department of Physics, Hong Kong Baptist University, Hong Kong SAR, China*
[3]*Division of Science, Engineering and Health Studies, College of Professional and Continuing Education,*
Hong Kong Polytechnic University, Hong Kong SAR, China

Unidirectional reflectionless resonance observed in parity-time-symmetric systems suggests a promising strategy to produce extremely asymmetric scattering. Inspired by such a unique feature, we propose a single-sided acoustic beam splitter that splits sound incident from a specific side but is totally transparent for sound incident from the opposite side. The unidirectional response is due to a parity-time-symmetric refractive index distribution. At the exceptional point when the real-part index and gain/loss modulations are balanced, it interacts with obliquely incident waves in a single-sided manner. In addition, by engineering the sidewall boundaries within an acoustic waveguide, we provide a general approach for obtaining the required complex refractive index, in which we show that the resistive or reactive component of the sidewall impedance can independently modulate the gain/loss or the real-part index. Based on this, a planar waveguide implementation of the single-sided acoustic beam splitter is demonstrated. Our study presents opportunities enabled by exploiting parity-time-symmetric systems in a higher-dimensional space and could find applications such as sensing and communication in a wide range of wave systems including but not limited to acoustics.

I. INTRODUCTION

A beam splitter can separate an incident beam into two or more beams that inherit the basic properties of the original beam (e.g., polarization, phase, and wavelength, etc.). It is frequently used as a key and primary element in applications such as interferometers and autocorrelators across a wide range of classical wave systems from electromagnetic waves to acoustic waves. Recent advances in acoustic artificial structures have stimulated a series of studies towards efficient splitting of sound, including designs based on conventional [1–3] or topological [4–6] phononic crystals, zero-index metamaterials [7,8], and acoustic metasurfaces [9–11]. Several related functional devices, for instance, acoustic Mach-Zehnder interferometer [12] and logic gates [13], have also been developed. However, it is still challenging to switch off the splitting effect on one side while keeping the other one unchanged. Such single-sided beam splitting requires extreme asymmetry in the scattering behavior, not available with previous symmetric configurations. The only existing work in this direction, although creative, is built around unidirectional mode conversion (from even to odd mode) and selection [14]. This gives rise to a difference in mode shape between the input and output that requires additional devices to recover the field pattern in practice.

The unique scattering properties of parity-time-symmetric (PT-symmetric) systems with exceptional points indicate a possible solution to the problem. PT symmetry is a concept that originated from non-Hermitian quantum theory, which describes a class of non-Hermitian Hamiltonians that commute with the combined parity and time-reversal operators [15]. It has been extensively explored in various classical wave systems through carefully engineered gain and/or loss [16–20], including the emerging PT-symmetric acoustics [21–39]. Remarkably, the existence of non-Hermitian degeneracies in this type of system, namely the so-called exceptional points where two or more eigenstates coalesce into one, leads to a variety of exotic phenomena and valuable functionalities. Among them, unidirectional invisibility or reflectionlessness (also known as anisotropic transmission resonance) is a hallmark of PT-symmetric scattering systems [40–42], in which vanishing reflection from one side together with strong or even enhanced reflection from the other side takes place near exceptional points defined by the generalized conservation relation. This effect has been theoretically and experimentally investigated as well in the realm of acoustics [21–23,27,28,43–49]. It could potentially serve as an ideal strategy for single-sided acoustic beam splitting when the input and output ports are arranged along different directions.

In this work, by taking advantage of the unidirectional reflectionless resonance supported by PT-symmetric systems, we report a multilayered structure that behaves as an acoustic beam splitter for sound incident from one side yet is fully transparent for opposite incidence, which distinguishes it from previous works that totally block the unsplit side. This structure has a PT-symmetric complex refractive index distribution. When an exceptional point is reached under balanced real and imaginary part modulations, it offers a unidirectional wave vector, thereby leading to extremely asymmetric scattering for oblique incidence. We then propose a general strategy exploiting sidewall impedance of an acoustic waveguide to

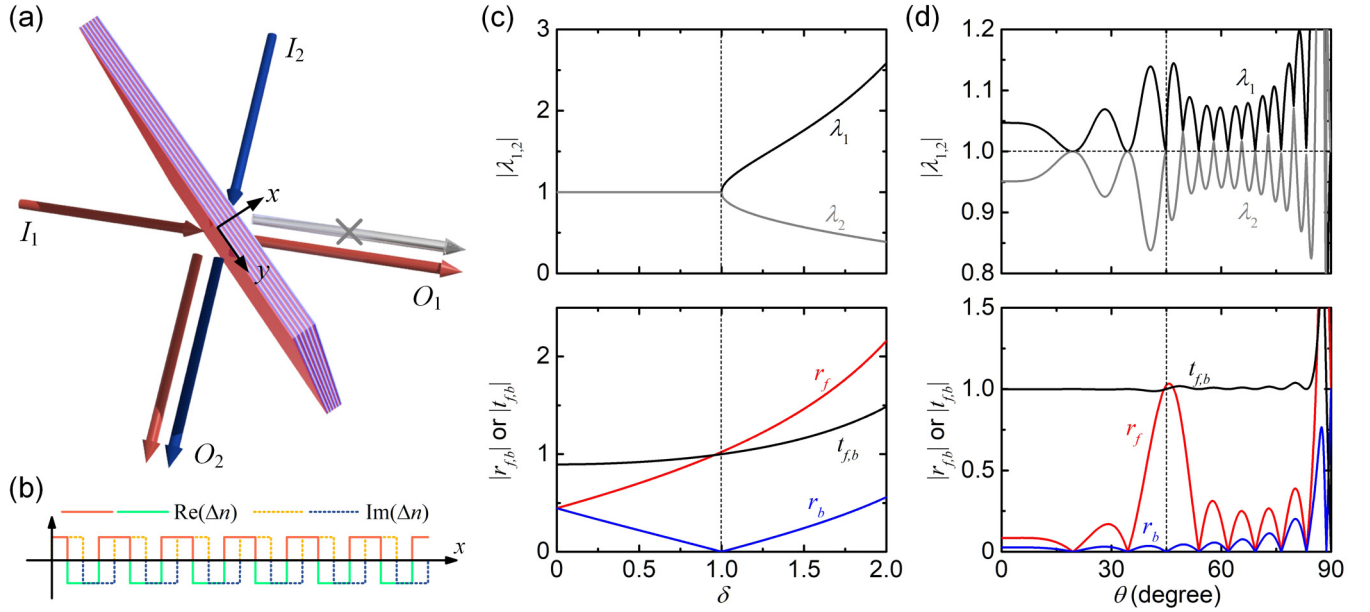*Corresponding author: jiezhu@polyu.edu.hk

FIG. 1. Exceptional-point-induced extremely asymmetric scattering for oblique incidence. (a) Schematic of the PT-symmetric multilayered structure. The structure is transparent to incident acoustic waves from I_2 (blue and white arrows) but works as a beam splitter for those from I_1 (red arrows). (b) PT-symmetric refractive index distribution along the x direction. (c) Scattering properties as a function of the imaginary-to-real part ratio with fixed $\theta = 45°$ and (d) as a function of the incident angle with fixed $\delta = 1$. Upper panels: absolute value of the eigenvalues of the beam-splitter matrix. Lower panels: reflection and transmission coefficients. The dashed lines indicate the position of the exceptional pint. The background medium is air with $\rho_0 = 1.21 \, \text{kg/m}^3$ and $c_0 = 343 \, \text{m/s}$; other parameters used in the calculation are $n' = 0.02n_0$, $4l = 50 \, \text{mm}$, $N_m = 6$, and $k_0 = \pi/4l \cos 45° \text{m}^{-1}$ that satisfies the wave-vector matching condition $\mathbf{q} + \mathbf{k}_i = \mathbf{k}_r$ with $|\mathbf{k}_i| = |\mathbf{k}_r| = k_0$ when $\delta = 1$ and $\theta = 45°$.

modulate the effective refractive index in the complex plane. It is subsequently applied to a planar waveguide implementation and demonstration of exceptional-point-induced single-sided acoustic beam splitting. Our results provide a possible route towards practical application of acoustic PT-symmetric systems, which may also benefit other classical wave systems.

II. THEORETICAL MODEL

As depicted in Figs. 1(a) and 1(b), the proposed single-sided acoustic beam splitter is a multilayered structure that can be described by a PT-symmetric refractive index modulation $n_0 + \Delta n(x)$ with

$$\Delta n(x) = \begin{cases} n'(1 + i\delta), & 4ml - 4l \leqslant x < 4ml - 3l \\ n'(-1 + i\delta), & 4ml - 3l \leqslant x < 4ml - 2l \\ n'(-1 - i\delta), & 4ml - 2l \leqslant x < 4ml - l \\ n'(1 - i\delta), & 4ml - l \leqslant x < 4ml \end{cases}, m = 1, 2, ..., N_m, \quad (1)$$

where n_0 is the background refractive index (both inside and outside the structure region), n' is the modulation amplitude ($n' \ll n_0$), i is the imaginary unit, δ is the imaginary-to-real-part ratio, $4l$ is the modulation period, and N_m is the total number of periods.

We consider an oblique plane-wave incidence from $x < 0$ in the xy plane [Fig. 1(a)]. The structure is homogeneous and infinitely extended in the transverse dimensions (y and z), and thus only the zeroth-order reflection and transmission are taken into account. The incident, reflected, and transmitted acoustic waves outside the structure can be written as $p_i e^{-ik_0 \cos \theta_i x} e^{-ik_0 \sin \theta_i y}$, $p_r e^{ik_0 \cos \theta_r x} e^{-ik_0 \sin \theta_r y}$, and $p_t e^{-ik_0 \cos \theta_t x} e^{-ik_0 \sin \theta_t y}$, respectively (the time dependency $e^{i\omega t}$ is omitted with ω being the angular frequency), in which k_0 is the background wave number, $p_{i,r,t}$ are the pressure amplitudes, $\theta_{i,r,t}$ are the angles, and the subscripts denote the in-

cidence, reflection, or transmission. The conservation of momentum in the y direction yields $k_y = k_0 \sin \theta_i = k_0 \sin \theta_r = k_0 \sin \theta_t$ and $\theta_i = \theta_r = \theta_t = \theta$. Accordingly, the acoustic pressure and the associated x-component particle velocity at $x < 0$ take the form

$$P = p_i e^{-ik_x x} e^{-ik_y y} + p_r e^{ik_x x} e^{-ik_y y}, \quad (2)$$

$$V_x = -\frac{1}{i\omega \rho_0} \frac{\partial P}{\partial x} = \frac{\cos \theta}{Z_0} p_i e^{-ik_x x} e^{-ik_y y} - \frac{\cos \theta}{Z_0} p_r e^{ik_x x} e^{-ik_y y}, \quad (3)$$

and the transmitted sound field at $x > 4lN_m$ reads

$$P = p_t e^{-ik_x x} e^{-ik_y y}, \quad (4)$$

$$V_x = \frac{\cos \theta}{Z_0} p_t e^{-ik_x x} e^{-ik_y y}, \quad (5)$$

where $Z_0 = \rho_0 c_0$ is the characteristic impedance, ρ_0 is the density, and c_0 is the speed of sound, respectively, of the background medium. Within each layer of the PT-symmetric modulation region $0 \leqslant x \leqslant 4lN_m$, the sound field can be expressed as the superposition of forward- and backward-propagating waves:

$$P = (A^{(m,j)}e^{-i\sqrt{k_j^2-k_y^2}x} + B^{(m,j)}e^{i\sqrt{k_j^2-k_y^2}x})e^{-ik_y y}, \quad (6)$$

$$V_x = \frac{\sqrt{k_j^2-k_y^2}}{k_j Z_j}(A^{(m,j)}e^{-i\sqrt{k_j^2-k_y^2}x} - B^{(m,j)}e^{i\sqrt{k_j^2-k_y^2}x})e^{-ik_y y}. \quad (7)$$

Here $A^{(m,j)}$ and $B^{(m,j)}$ represent the forward- and backward-propagating wave amplitudes in the jth layer ($j = 1, 2, 3, 4$) of the mth period. The corresponding characteristic impedance and wave number are $Z_j = \rho_0 c_j$ and $k_j = k_0 n_0^{-1} n(x)$, in which the density is the same as that of the background medium ρ_0 while the speed of sound varies with the PT-symmetric refractive index distribution as $c_j = \omega k_j^{-1}$.

The acoustic pressures and particle velocities at the two interfaces of each layer can be related through a 2×2 transfer matrix $\mathbf{T}_j$ in the form

$$\begin{bmatrix} P \\ V_x \end{bmatrix}\bigg|_{x=(j-1)l} = \mathbf{T}_j \cdot \begin{bmatrix} P \\ V_x \end{bmatrix}\bigg|_{x=jl}, \quad (8)$$

and the components are determined from Eqs. (6) and (7) as

$$\mathbf{T}_j = \begin{bmatrix} \cos(k_j l) & i\frac{k_j Z_j}{\sqrt{k_j^2-k_y^2}}\sin(k_j l) \\ i\frac{\sqrt{k_j^2-k_y^2}}{k_j Z_j}\sin(k_j l) & \cos(k_j l) \end{bmatrix}. \quad (9)$$

Applying the relation to the entire multilayered system extending from $x = 0$ to $x = 4lN_m$, one has

$$\begin{bmatrix} P \\ V_x \end{bmatrix}\bigg|_{x=0} = \mathbf{T}_f \cdot \begin{bmatrix} P \\ V_x \end{bmatrix}\bigg|_{x=4lN_m}, \quad (10)$$

where

$$\mathbf{T}_f = [\mathbf{T}_1 \cdot \mathbf{T}_2 \cdot \mathbf{T}_3 \cdot \mathbf{T}_4]^{N_m} = \begin{bmatrix} T_{11} & T_{12} \\ T_{21} & T_{22} \end{bmatrix}. \quad (11)$$

The reflection and transmission coefficients for the forward incidence [I_1 in Fig. 1(a)] can then be derived as

$$r_f = \frac{p_r}{p_i} = \frac{T_{11} + (T_{12}\cos\theta/Z_0) - Z_0 T_{21}/\cos\theta - T_{22}}{T_{11} + (T_{12}\cos\theta/Z_0) + Z_0 T_{21}/\cos\theta + T_{22}}, \quad (12)$$

$$t_f = \frac{p_t}{p_i} = \frac{2e^{ik_0 4lN_m}}{T_{11} + (T_{12}\cos\theta/Z_0) + Z_0 T_{21}/\cos\theta + T_{22}}. \quad (13)$$

Regarding the backward incidence from $x > 4lN_m$ [I_2 in Fig. 1(a)], for simplicity, we consider a reversed arrangement of the multilayered structure. In this case, the overall transfer matrix as given in Eq. (11) becomes $\mathbf{T}_b = [\mathbf{T}_4 \cdot \mathbf{T}_3 \cdot \mathbf{T}_2 \cdot \mathbf{T}_1]^{N_m}$ so that the backward reflection r_b can be obtained in a similar way.

Now we define an input and an output on each side of the multilayered structure [see Fig. 1(a)]. In general, this four-port system allows both incoming and outgoing waves at each port and can be completely described by a 4×4 scattering matrix as

$$\begin{bmatrix} p_{I_1}^- \\ p_{I_2}^- \\ p_{O_1}^- \\ p_{O_2}^- \end{bmatrix} = \begin{bmatrix} S_{11} & S_{12} & S_{13} & S_{14} \\ S_{21} & S_{22} & S_{23} & S_{24} \\ S_{31} & S_{32} & S_{33} & S_{34} \\ S_{41} & S_{42} & S_{43} & S_{44} \end{bmatrix} \begin{bmatrix} p_{I_1}^+ \\ p_{I_2}^+ \\ p_{O_1}^+ \\ p_{O_2}^+ \end{bmatrix}, \quad (14)$$

where the subscript $I_{1,2}$ or $O_{1,2}$ represents the corresponding input or output port and the superscript $+$ or $-$ represents the incoming or outgoing wave of the system. Given that all higher-order diffraction modes are negligible and the presented structure is homogeneous along the y direction, an incident plane wave at one input (or output) port only produces one specular reflection and one direct transmission respectively appearing at the two output (or input) ports, with the paths being reversible. Therefore, the elements S_{11} to S_{22} and S_{33} to S_{44} of the scattering matrix are zero; other elements $S_{13} = S_{24} = S_{31} = S_{42} = t_f = t_b$, $S_{14} = S_{41} = r_f$, $S_{23} = S_{32} = r_b$. Equation (14) can thus be simplified as a 2×2 beam-splitter matrix if we only take into consideration
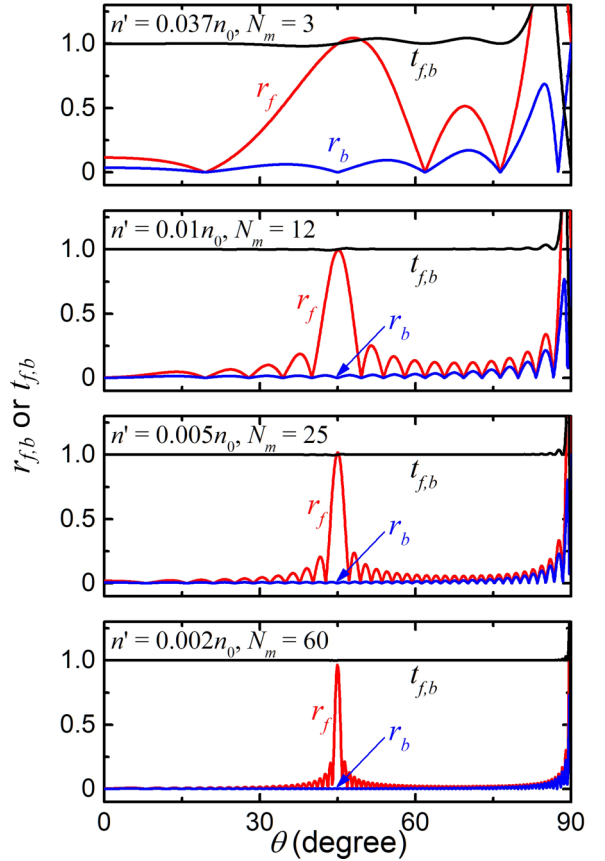

FIG. 2. Angular selectivity of the single-sided wave splitting effect for different modulation amplitudes and total numbers of periods. From top to bottom: $n' = 0.037n_0$ and $N_m = 3$; $n' = 0.01n_0$ and $N_m = 12$; $n' = 0.005n_0$ and $N_m = 25$; $n' = 0.002n_0$ and $N_m = 60$.

the incoming waves at the two input ports:

$$
\begin{bmatrix} p_{O_1}^- \\ p_{O_2}^- \end{bmatrix} = \begin{bmatrix} t & r_b \\ r_f & t \end{bmatrix} \begin{bmatrix} p_{I_1}^+ \\ p_{I_2}^+ \end{bmatrix}. \tag{15}
$$

Figure 1(c) displays an example with an incident angle of $\theta = 45°$, wherein an exceptional point arises in the parameter space at the Bragg resonance ($k_0 = \pi/4l \cos 45° \mathrm{m}^{-1}$), leading to the single-sided wave splitting effect. The parameters used in our calculation are listed in the caption of Fig. 1. It can be seen that the two eigenvalues of the beam-splitter matrix [upper panel in Fig. 1(c)], $\lambda_{1,2} = t \pm \sqrt{r_f r_b}$, experience a PT phase transition with the increase of the imaginary-to-real-part ratio δ. This transition behavior is governed by the generalized conservation relation $|T - 1| = \sqrt{R_f R_b}$ [40,41], where $R_{f,b} = |r_{f,b}|^2$ and $T = |t|^2$ are the reflectances and transmittance. For balanced real and imaginary part modulations ($\delta = 1$), $r_b = 0$ and $r_f \neq 0$ with $|t| = 1$ [lower panel in Fig. 1(d)] so that $\lambda_1 = \lambda_2$, which signifies the existence of an exceptional point of the scattering matrix. These results indicate that forward-incident waves will be split into two coherent output waves (one reflected and one transmitted along different directions), but backward-incident waves propagate through the structure without any scattering [40]. In other words, when operating at the exceptional point, the multilayered structure is able to work as a single-sided acoustic beam splitter. It can generate two output beams when a wave obliquely impinges from one side but allows scattering-free wave propagation with opposite incidence. It is noteworthy that a slight detuning of δ from the exceptional point will not fully eliminate the extreme asymmetry in reflection. Specific to our studied case [lower panel in Fig. 1(c)], in the range $0.9 < \delta < 1.1$, we have $r_b < 0.045$, $r_f > 0.951$, and $0.978 < t < 1.025$, which means

the single-sided beam splitting effect remains highly efficient in the vicinity of the exceptional point.

Alternatively, this single-sided wave splitting effect can be understood from the perspective of directional wave-vector matching. At the exceptional point ($\delta = 1$), the Fourier transform of Eq. (1) in reciprocal space contains a unidirectional wave vector of magnitude $|\mathbf{q}| = q = \pi/2l$, similar to that of a complex sinusoidal modulation $\cos(qx) + i \sin(qx)$ [28,37,40,42]. Strong reflection takes place when the wave-vector matching condition $\mathbf{q} + \mathbf{k}_i = \mathbf{k}_r$ with $|\mathbf{k}_i| = |\mathbf{k}_r| = k_0$ is satisfied, where $\mathbf{k}_i$ and $\mathbf{k}_r$ are the incident and reflected wave vectors. In the one-dimensional case, the structure interacts with a normal incident wave of wave vector $\mathbf{k}_i = -\mathbf{q}/2$ and gives rise to a reflected one of wave vector $\mathbf{k}_r = \mathbf{q}/2$, but not vice versa. For oblique incidence, the wave-vector matching becomes directional according to the rule of two-dimensional vector addition [28]. Hence, the wave splitting effect can be observed when the magnitude of the incident wave vector is $|\mathbf{k}_i| = |\mathbf{k}_r| = k_0 = q/2 \cos \theta$.

It then should be noted that the exceptional point is angle dependent. As shown in Fig. 1(d), the exceptional point appears at $\theta = 45°$, and there exist a series of trivial merging points caused by the bidirectional reflectionlessness. In addition, the backward reflection of the studied structure is rather weak upon most angles of incidence ($0 < \theta < 84.7°$, $R_b < 0.05$) except for grazing incidence. As a result, the wave splitting effect is valid in a certain angular range (full width at half maximum $\sim 8.7°$), but the trivial scattering peaks in the forward direction associated with the total number of periods N_m are relatively remarkable compared to those in the backward direction.

The overall thickness of the proposed beam splitter can be reduced at the expenses of decreased angular selectivity
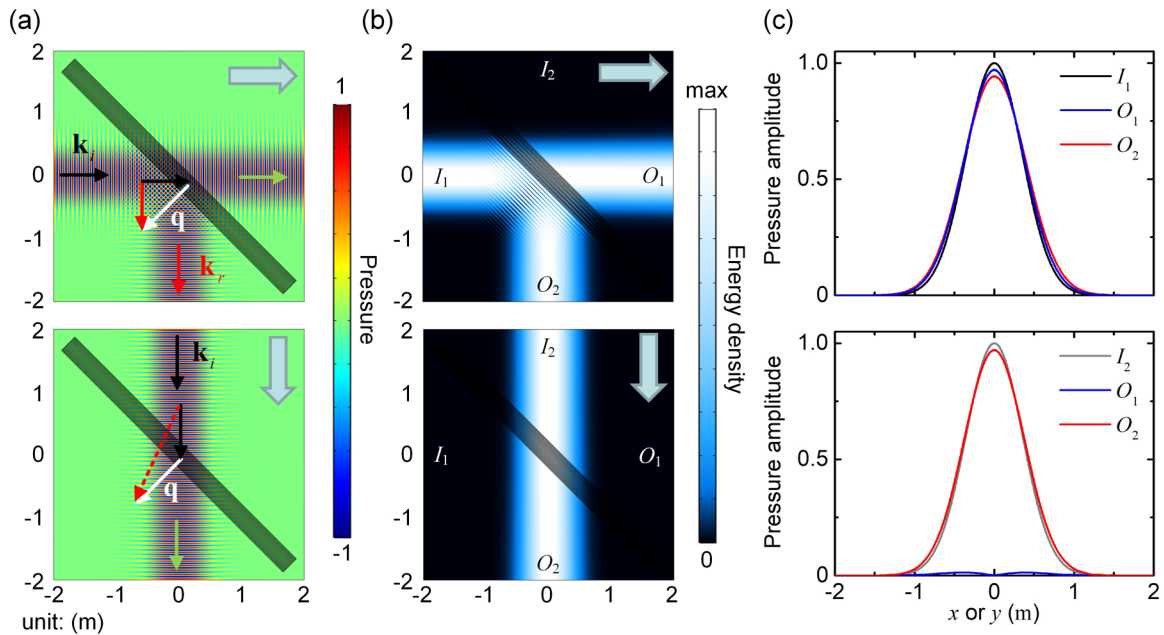

FIG. 3. Numerical simulation of the single-sided acoustic beam splitting effect. Simulated (a) acoustic pressure and (b) energy density fields. The thick arrows denote the incident directions. The thin arrows denote the incident (black), reflected (red), transmitted (green) and exceptional-point-induced unidirectional (white) wave vectors. (c) Pressure amplitude distributions at the input and output ports. Upper panels: incidence from I_1. Lower panels: incidence from I_2. The parameters are the same as those given in the caption of Fig. 1 with fixed $\delta = 1$ and $\theta = 45°$.

and increased sidelobe (uppermost panel in Fig. 2). Inversely, to further improve the angular selectivity and suppress the sidelobes, we may employ a larger number of modulation periods N_m and a smaller modulation amplitude n'. As can be seen in Fig. 2, an increased N_m with simultaneously decreased n' clearly results in a sharper reflection peak, e.g., for the case of $n' = 0.005n_0$ and $N_m = 25$, the full width at half maximum is about $2°$. Note that decreasing n' guarantees an approximately unchanged reflectance, which also helps to inhibit the trivial scattering despite that the weak modulation is sensitive to errors in practice.

We verify our idea and the transfer matrix modeling by numerically examining the interaction of an ideal PT-symmetric multilayered structure at its exceptional point with obliquely incident acoustic beams from both sides. The full-wave simulations here (and throughout this paper) were performed in COMSOL Multiphysics. The parameters are the same as those presented in the caption of Fig. 1. For convenience, a $45°$ counterclockwise rotation is applied to the structure so that the two input ports I_1 and I_2 are defined as the left and top boundaries, respectively. The structure has a lateral dimension of 5 m, which is much larger than the beam waist 0.5 m. As shown in the simulated acoustic pressure and energy density fields, the incident beam from I_1 [upper panels, Figs. 3(a) and 3(b)] is split into a transmitted one propagating along the same direction and a strong downward reflection, reaching the two output ports O_1 and O_2, whereas for the incidence from I_2 [lower panels, Figs. 3(a) and 3(b)], the beam penetrates the structure and then continues to propagate to the output port O_2 with no scattering and no change in either amplitude or wave form, which means that the structure is almost fully transparent. The thin arrows in Fig. 3(a) intuitively illustrate how the wave-vector matching occurs ($I_1 : \mathbf{q} + \mathbf{k}_i = \mathbf{k}_r$ and $I_2 : \mathbf{q} + \mathbf{k}_i \neq \mathbf{k}_r$) and consequently leads to the single-sided beam splitting effect. The extracted pressure amplitude distributions at the input and output ports as given in Fig. 3(c) are consistent with the theoretical predictions of Fig. 1(d) and further confirm the extreme asymmetry in reflection. It is seen that the beam's central amplitude decreases slightly which is caused by the spreading of the beam in the lateral direction.

III. MODULATING THE COMPLEX REFRACTIVE INDEX WITHIN A WAVEGUIDE

The complex refractive index distribution as given by Eq. (1) involves weak modulation of the real and imaginary parts (a slight deviation of the refractive index Δn from the background refractive index n_0), which respectively correspond to the effective wave speed and the energy exchange with the external. This can be realized by altering the sidewall impedance $Z = R + iX$ (or admittance $Y = Z^{-1}$) inside an acoustic waveguide [see Fig. 4(a)], where R and X are the acoustic resistance and reactance. The variation in the reactance of the sidewall impedance decelerates or accelerates the sound waves (fundamental mode) travelling along the waveguide, thereby tuning the real-part refractive index. On the other hand, the sidewall impedance's resistive component determines the acoustic energy injected to or taken away from the waveguide during propagation and thus introduces the imaginary part to the effective refractive index.
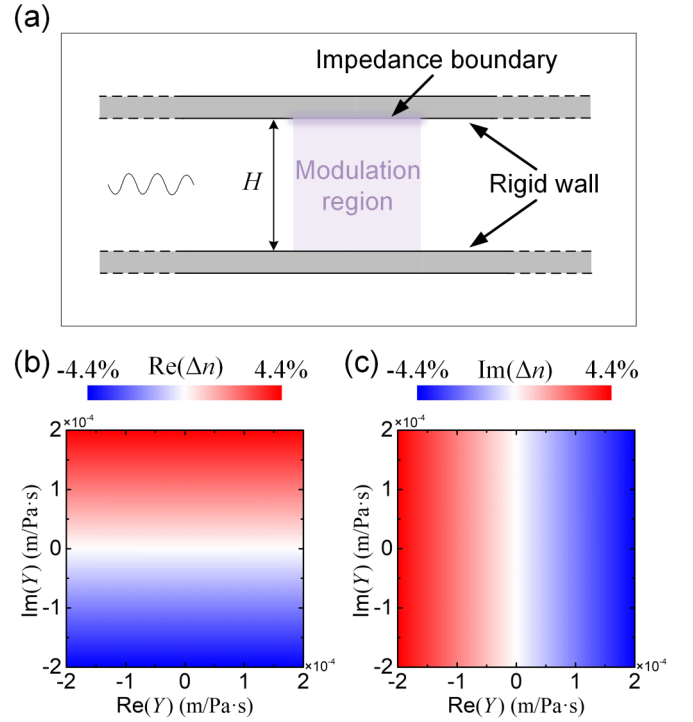

FIG. 4. Complex refractive index modulation within an acoustic waveguide. (a) Schematic of the acoustic waveguide with a sidewall impedance boundary. The sidewalls are rigid except for the upper boundary of the modulated region. (b) Real and (c) imaginary parts of the variation in the retrieved effective refractive index as functions of the sidewall admittance. In the calculation, $H = 15$ mm, $D = 25$ mm, and the frequency is $f = 4850.8$ Hz.

We provide two groups of numerical results to confirm the aforementioned modulation approach. The height of the acoustic waveguide is $H = 15$ mm, the length of the modulation region is $D = 25$ mm, and the studied frequency is $f = 4850.8$ Hz corresponding to the Bragg resonance in Figs. 1–3. The reflection and transmission coefficients of the modulation region were first obtained in full-wave simulations and then used to extract the effective properties based on a standard retrieval method [50]. Here the swept parameter is the admittance $Y = Z^{-1}$ rather than the impedance itself for ease of presentation, since the weak modulation ($\Delta n \ll n_0$) requires a small variation of Y around zero. As can be observed from Figs. 4(b) and 4(c), varying the imaginary (real) part of Y results in subtle change in only the real (imaginary) part of the refractive index, without affecting the other. This suggests that the real and imaginary parts of the refractive index are decoupled for weak modulation in our approach and can be well tailored independently to meet the requirement of a PT-symmetric refractive index distribution.

IV. PLANAR WAVEGUIDE IMPLEMENTATION

With the modulation approach mentioned above, we present an artificial-boundary-based planar waveguide implementation of the PT-symmetric acoustic beam splitter. The arrangement of the sidewall impedance boundaries along the cross section of the planar waveguide ($H = 15$ mm) is
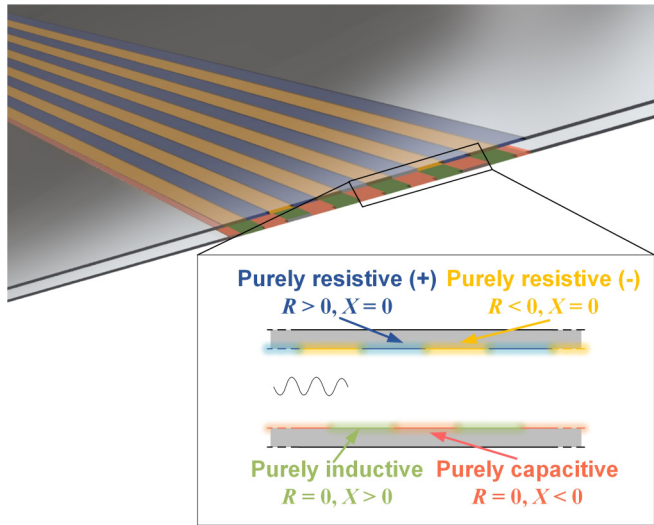
FIG. 5. Schematic of the planar acoustic waveguide implementation. The four colors represent four different types of artificial boundary conditions that correspond to the independent real and imaginary part modulations of the refractive index (including both positive and negative values).

schematically illustrated in Fig. 5. Purely inductive ($R = 0$, $X = 10\,526\,\mathrm{Pa\,m/s}$) and purely capacitive ($R = 0$, $X = -10\,526\,\mathrm{Pa\,m/s}$) boundaries are periodically interleaved on the bottom wall to modulate the real part of the refractive index; and two types of purely resistive boundaries ($R = 10\,526\,\mathrm{Pa\,m/s}$, $X = 0$ and $R = -10\,526\,\mathrm{Pa\,m/s}$, $X = 0$) decorated similarly on the top wall are able to provide the loss and gain. They are combined in a quarter-period-shifted manner according to the complex refractive index distribution of the

single-sided acoustic beam splitter as described in the caption of Fig. 3.

The simulation results of the designed planar waveguide are shown in Fig. 6. They agree well with both our theoretical prediction [see Figs. 1(b) and 1(c)] and numerical results (see Fig. 3). We observe that the modulated region of the waveguide is able to separate the incident beam from I_1 into two output beams with nearly identical amplitude. In contrast, the beam incident from I_2 goes through the modulated region without any scattering or distortion. These simulation results evidently validate that our design can be used to realize the PT-symmetric single-sided beam splitter.

Experimental realization of on-demand complex surface acoustic impedance is rather challenging yet still possible. Metamaterial structures such as subwavelength periodic grooves or Helmholtz resonators array [28,48] are ideal candidates for the reactive boundaries. When operating off resonance, they offer dominantly either capacitive or inductive boundary condition that is macroscopically homogeneous. Resistive boundaries concerning loss effect ($R > 0$) can be achieved through introducing leakage or dissipation via microperforated plates [37], mesh fabrics [28,38], or subwavelength resonant absorbers [35,51,52]. Meanwhile, acoustic gain ($R < 0$) is possible with active electroacoustic components such as virtual atoms or loudspeakers with external circuit [22,31,35,53]. Specific to the studied waveguide configuration, an assembly of subwavelength microloudspeaker units, albeit very complicated to implement, may be embedded into the sidewalls to mimic the negative resistive boundaries. It is worth mentioning that, even if the artificial structures are not as ideal as we expected, the unidirectional reflectionlessness can still be achieved since the square-wave index profile presented in our study is one among many ways to construct an exceptional point of the scattering matrix.
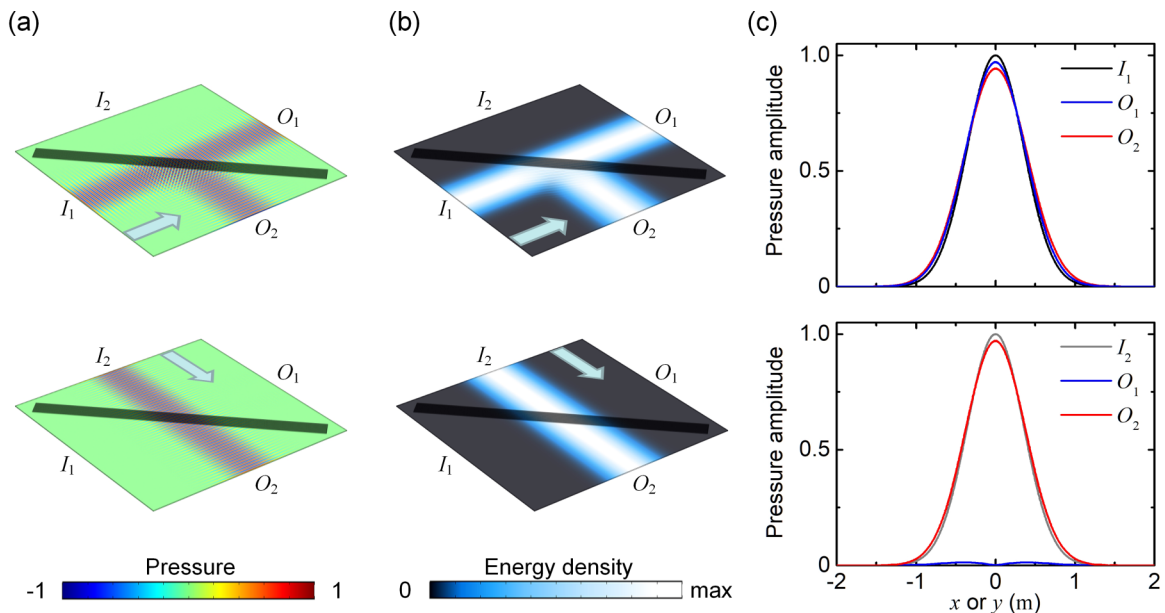

FIG. 6. Numerical simulation of the planar waveguide implementation of the PT-symmetric single-sided acoustic beam splitter. Simulated (a) acoustic pressure and (b) energy density fields. The thick arrows denote the incident directions. (c) Pressure amplitude distributions at the input and output ports. Upper panels: incidence from I_1. Lower panels: incidence from I_2.

The impedance boundary in each layer does not necessarily have to be homogeneous and span the entire layer [37]. A complex refractive index modulation is able to provide a unidirectional wave vector as long as its Fourier expansions contain the component $\cos(qx) + i\sin(qx)$. Other than the artificial structures for quiescent media, acoustic liners may be an alternative approach to the required complex refractive index distribution in the presence of flow [54,55].

V. CONCLUSIONS

To conclude, we have proposed a single-sided acoustic beam splitter together with its planar waveguide implementation. The device is based on the extremely asymmetric scattering properties introduced by a PT-symmetric multilayered structure at the exceptional point. In addition to the unidirectional wave splitting effect, the presented design is completely transparent from the unsplit side, which is an important feature not accessible in previous designs. A general approach to the complex refractive index modulation has also been discussed and subsequently applied to the waveguide realization. By considering obliquely incident waves, we show that PT-symmetric systems bring exciting possibilities towards extraordinary sound manipulation, which may benefit unconventional devices for high-performance acoustic sensing and communication.

[1] J. Bucay, E. Roussel, J. O. Vasseur, P. A. Deymier, A. C. Hladky-Hennion, Y. Pennec, K. Muralidharan, B. Djafari-Rouhani, and B. Dubus, Positive, negative, zero refraction, and beam splitting in a solid/air phononic crystal: Theoretical and experimental study, Phys. Rev. B **79**, 214305 (2009).

[2] B. Li, J. J. Guan, K. Deng, and H. P. Zhao, Splitting of self-collimated beams in two-dimensional sonic crystals, J. Appl. Phys. **112**, 124514 (2012).

[3] J. Li, F. G. Wu, H. L. Zhong, Y. W. Yao, and X. Zhang, Acoustic beam splitting in two-dimensional phononic crystals using self-collimation effect, J. Appl. Phys. **118**, 144903 (2015).

[4] C. He, X. Ni, H. Ge, X.-C. Sun, Y.-B. Chen, M.-H. Lu, X.-P. Liu, and Y.-F. Chen, Acoustic topological insulator and robust one-way sound transport, Nat. Phys. **12**, 1124 (2016).

[5] L. P. Ye, C. Y. Qiu, J. Y. Lu, X. H. Wen, Y. Y. Shen, M. Z. Ke, F. Zhang, and Z. Y. Liu, Observation of acoustic valley vortex states and valley-chirality locked beam splitting, Phys. Rev. B **95**, 174106 (2017).

[6] Z. X. Zhu, X. Q. Huang, J. Y. Lu, M. Yan, F. Li, W. Y. Deng, and Z. Y. Liu, Negative Refraction and Partition in Acoustic Valley Materials of a Square Lattice, Phys. Rev. Appl. **12**, 024007 (2019).

[7] R. Graciá-Salgado, V. M. García-Chocano, D. Torrent, and J. Sánchez-Dehesa, Negative mass density and ρ-near-zero quasi-two-dimensional metamaterials: Design and applications, Phys. Rev. B **88**, 224305 (2013).

[8] X. X. Yan, W. Wei, N. Hu, and F. M. Liu, Splitting of acoustic energy by zero index metamaterials, Phys. Lett. A **379**, 2147 (2015).

[9] X. S. Fang, X. Wang, and Y. Li, Acoustic Splitting and Bending with Compact Coding Metasurfaces, Phys. Rev. Appl. **11**, 064033 (2019).

[10] H. Q. Ni, X. S. Fang, Z. L. Hou, Y. Li, and B. Assouar, High-efficiency anomalous splitter by acoustic meta-grating, Phys. Rev. B **100**, 104104 (2019).

[11] S. T. Cao and Z. L. Hou, Angular-Asymmetric Transmitting Metasurface and Splitter for Acoustic Waves: Combining the Coherent Perfect Absorber and a Laser, Phys. Rev. Appl. **12**, 064016 (2019).

[12] O. A. Kaya, A. Cicek, A. Salman, and B. Ulug, Acoustic Mach–Zehnder interferometer utilizing self-collimated beams

in a two-dimensional phononic crystal, Sens. Actuators, B **203**, 197 (2014).

[13] T. Zhang, Y. Cheng, J. Z. Guo, J. Y. Xu, and X. J. Liu, Acoustic logic gates and Boolean operation based on self-collimating acoustic beams, Appl. Phys. Lett. **106**, 113503 (2015).

[14] Y. Tang, Y. Zhu, B. Liang, J. Yang, J. Yang, and J. Cheng, One-way Acoustic Beam Splitter, Sci. Rep. **8**, 13573 (2018).

[15] C. M. Bender and S. Boettcher, Real spectra in non-Hermitian Hamiltonians having PT symmetry, Phys. Rev. Lett. **80**, 5243 (1998).

[16] L. Feng, R. El-Ganainy, and L. Ge, Non-Hermitian photonics based on parity-time symmetry, Nat. Photon. **11**, 752 (2017).

[17] R. El-Ganainy, K. G. Makris, M. Khajavikhan, Z. H. Musslimani, S. Rotter, and D. N. Christodoulides, Non-Hermitian physics and PT symmetry, Nat. Phys. **14**, 11 (2018).

[18] H. Zhao and L. Feng, Parity-time symmetric photonics, Natl. Sci. Rev. **5**, 183 (2018).

[19] M. A. Miri and A. Alu, Exceptional points in optics and photonics, Science **363**, eaar7709 (2019).

[20] S. K. Ozdemir, S. Rotter, F. Nori, and L. Yang, Parity-time symmetry and exceptional points in photonics, Nat. Mater. **18**, 783 (2019).

[21] X. F. Zhu, H. Ramezani, C. Z. Shi, J. Zhu, and X. Zhang, PT-Symmetric Acoustics, Phys. Rev. X **4**, 031042 (2014).

[22] R. Fleury, D. Sounas, and A. Alu, An invisible acoustic sensor based on parity-time symmetry, Nat. Commun. **6**, 5905 (2015).

[23] C. Shi, M. Dubois, Y. Chen, L. Cheng, H. Ramezani, Y. Wang, and X. Zhang, Accessing the exceptional points of parity-time symmetric acoustics, Nat. Commun. **7**, 11110 (2016).

[24] J. Christensen, M. Willatzen, V. R. Velasco, and M. H. Lu, Parity-Time Synthetic Phononic Media, Phys. Rev. Lett. **116**, 207601 (2016).

[25] K. Ding, G. C. Ma, M. Xiao, Z. Q. Zhang, and C. T. Chan, Emergence, Coalescence, and Topological Properties of Multiple Exceptional Points and their Experimental Realization, Phys. Rev. X **6**, 021007 (2016).

[26] V. Achilleos, G. Theocharis, O. Richoux, and V. Pagneux, Non-Hermitian acoustic metamaterials: Role of exceptional points in sound absorption, Phys. Rev. B **95**, 144303 (2017).

[27] Y. Auregan and V. Pagneux, PT-Symmetric Scattering in Flow Duct Acoustics, Phys. Rev. Lett. **118**, 174301 (2017).

[28] T. Liu, X. Zhu, F. Chen, S. Liang, and J. Zhu, Unidirectional Wave Vector Manipulation in Two-Dimensional Space with an all Passive Acoustic Parity-Time-Symmetric Metamaterials Crystal, Phys. Rev. Lett. **120**, 124502 (2018).

[29] M. Wang, L. Ye, J. Christensen, and Z. Liu, Valley Physics in non-Hermitian Artificial Acoustic Boron Nitride, Phys. Rev. Lett. **120**, 246601 (2018).

[30] K. Ding, G. Ma, Z. Q. Zhang, and C. T. Chan, Experimental Demonstration of an Anisotropic Exceptional Point, Phys. Rev. Lett. **121**, 085702 (2018).

[31] E. Rivet, A. Brandstotter, K. G. Makris, H. Lissek, S. Rotter, and R. Fleury, Constant-pressure sound waves in non-Hermitian disordered media, Nat. Phys. **14**, 942 (2018).

[32] Y. Q. Liu, Z. X. Liang, J. Zhu, L. B. Xia, O. Mondain-Monval, T. Brunet, A. Alu, and J. S. Li, Willis Metamaterial on a Structured Beam, Phys. Rev. X **9**, 011040 (2019).

[33] W. Q. Ji, Q. Wei, X. F. Zhu, D. J. Wu, and X. J. Liu, Extraordinary acoustic scattering in a periodic PT-symmetric zero-index metamaterials waveguide, Europhys. Lett. **125**, 58002 (2019).

[34] Z. Zhang, M. Rosendo Lopez, Y. Cheng, X. Liu, and J. Christensen, Non-Hermitian Sonic Second-Order Topological Insulator, Phys. Rev. Lett. **122**, 195501 (2019).

[35] H. X. Li, M. Rosendo-López, Y.-F. Zhu, X.-D. Fan, D. Torrent, B. Liang, J.-C. Cheng, and J. Christensen, Ultrathin acoustic parity-time symmetric metasurface cloak, Research **2019**, 8345683 (2019).

[36] X. Wang, X. Fang, D. Mao, Y. Jing, and Y. Li, Extremely Asymmetrical Acoustic Metasurface Mirror at the Exceptional Point, Phys. Rev. Lett. **123**, 214302 (2019).

[37] H. Z. Chen, T. Liu, H. Y. Luan, R. J. Liu, X. Y. Wang, X. F. Zhu, Y. B. Li, Z. M. Gu, S. J. Liang, H. Gao, L. Lu, L. Ge, S. Zhang, J. Zhu, and R. M. Ma, Revealing the missing dimension at an exceptional point, Nat. Phys. **16**, 571 (2020).

[38] J. Lan, L. W. Wang, X. W. Zhang, M. H. Lu, and X. Z. Liu, Acoustic Multifunctional Logic Gates and Amplifier Based on Passive Parity-Time Symmetry, Phys. Rev. Appl. **13**, 034047 (2020).

[39] H. Gao, H. Xue, Q. Wang, Z. Gu, T. Liu, J. Zhu, and B. Zhang, Observation of topological edge states induced solely by non-Hermiticity in an acoustic crystal, Phys. Rev. B **101**, 180303 (2020).

[40] Z. Lin, H. Ramezani, T. Eichelkraut, T. Kottos, H. Cao, and D. N. Christodoulides, Unidirectional Invisibility Induced by PT-Symmetric Periodic Structures, Phys. Rev. Lett. **106**, 213901 (2011).

[41] L. Ge, Y. D. Chong, and A. D. Stone, Conservation relations and anisotropic transmission resonances in one-dimensional PT-

symmetric photonic heterostructures, Phys. Rev. A **85**, 023802 (2012).

[42] L. Feng, Y. L. Xu, W. S. Fegadolli, M. H. Lu, J. E. Oliveira, V. R. Almeida, Y. F. Chen, and A. Scherer, Experimental demonstration of a unidirectional reflectionless parity-time metamaterial at optical frequencies, Nat. Mater. **12**, 108 (2013).

[43] D. G. Zhao, Y. X. Shen, Y. Zhang, X. F. Zhu, and L. Yi, Bound states in one-dimensional acoustic parity-time-symmetric lattices for perfect sensing, Phys. Lett. A **380**, 2698 (2016).

[44] W. Zhu, X. Fang, D. Li, Y. Sun, Y. Li, Y. Jing, and H. Chen, Simultaneous Observation of a Topological Edge State and Exceptional Point in an Open and Non-Hermitian Acoustic System, Phys. Rev. Lett. **121**, 124501 (2018).

[45] A. Merkel, V. Romero-Garcia, J. P. Groby, J. Li, and J. Christensen, Unidirectional zero sonic reflection in passive PT-symmetric Willis media, Phys. Rev. B **98**, 201102 (2018).

[46] C. Shen, J. F. Li, X. Y. Peng, and S. A. Cummer, Synthetic exceptional points and unidirectional zero reflection in non-Hermitian acoustic systems, Phys. Rev. Mater. **2**, 125203 (2018).

[47] M. Rosendo-López, A. Merkel, and J. Christensen, PT-symmetric sonic crystals: From asymmetric echoes to supersonic speeds, Europhys. Lett. **124**, 34001 (2018).

[48] Y. Z. Yang, H. Jia, Y. F. Bi, H. Zhao, and J. Yang, Experimental Demonstration of an Acoustic Asymmetric Diffraction Grating Based on Passive Parity-Time-Symmetric Medium, Phys. Rev. Appl. **12**, 034040 (2019).

[49] Q. Wu, Y. Chen, and G. Huang, Asymmetric scattering of flexural waves in a parity-time symmetric metamaterial beam, J. Acoust. Soc. Am. **146**, 850 (2019).

[50] V. Fokin, M. Ambati, C. Sun, and X. Zhang, Method for retrieving effective properties of locally resonant acoustic metamaterials, Phys. Rev. B **76**, 144302 (2007).

[51] R. Zhao, T. Liu, C. Y. Wen, J. Zhu, and L. Cheng, Impedance-Near-Zero Acoustic Metasurface for Hypersonic Boundary-Layer Flow Stabilization, Phys. Rev. Appl. **11**, 044015 (2019).

[52] S. Huang, Z. Zhou, D. Li, T. Liu, X. Wang, J. Zhu, and Y. Li, Compact broadband acoustic sink with coherently coupled weak resonances, Sci. Bull. **65**, 373 (2020).

[53] C. Cho, X. Wen, N. Park, and J. Li, Digitally virtualized atoms for acoustic metamaterials, Nat. Commun. **11**, 251 (2020).

[54] Y. Auregan and V. Pagneux, Slow sound in lined flow ducts, J. Acoust. Soc. Am. **138**, 605 (2015).

[55] A. Coutant, Y. Auregan, and V. Pagneux, Slow sound laser in lined flow ducts, J. Acoust. Soc. Am. **146**, 2632 (2019).